

Climate change drives record-breaking heat in Iceland and Greenland challenging cold adapted ecosystems and societies

Authors

Sarah Kew, *Royal Netherlands Meteorological Institute (KNMI), De Bilt, The Netherlands*
Caroline Drost Jensen, *Danish Meteorological Institute (DMI), Copenhagen, Denmark*
Halldór Björnsson, *Icelandic Met Office (IMO), Reykjavik, Iceland*
Izidine Pinto, *Royal Netherlands Meteorological Institute (KNMI), De Bilt, The Netherlands*
Sjoukje Philip, *Royal Netherlands Meteorological Institute (KNMI), De Bilt, The Netherlands*
Maja Vahlberg, *Red Cross Red Crescent Climate Centre, The Hague, the Netherlands; Swedish Red Cross, Stockholm, Sweden (based in Umeå/Umeå, Sweden)*
Vikki Thompson, *Royal Netherlands Meteorological Institute (KNMI), De Bilt, The Netherlands*
Clair Barnes, *Centre for Environmental Policy, Imperial College, London, UK*
Ben Clarke, *Centre for Environmental Policy, Imperial College, London, UK*
Thomas Gravggaard Askjær, *Danish Meteorological Institute (DMI), Copenhagen, Denmark*
Nick Baumgart, *Copenhagen Centre for Disaster Research, Global Health Section, Department of Public Health, University of Copenhagen, Copenhagen, Denmark*
Emmanuel Raju, *Copenhagen Centre for Disaster Research, Global Health Section, Department of Public Health, University of Copenhagen, Copenhagen, Denmark; African Centre for Disaster Studies, North-West University, South Africa*
Miriam Cullen, *Centre for European, Comparative, and Constitutional Legal Studies, Faculty of Law, University of Copenhagen, Copenhagen, Denmark*
Friederike Otto, *Centre for Environmental Policy, Imperial College, London, UK*

Review authors

Friederike Otto, *Centre for Environmental Policy, Imperial College, London, UK*
Mariam Zachariah, *Centre for Environmental Policy, Imperial College, London, UK*
Roop Singh, *Red Cross Red Crescent Climate Centre, The Hague, the Netherlands (based in New Jersey, USA)*
Paula Haro, *Regional Office for Europe, International Federation of the Red Cross and Red Crescent Societies (IFRC), Budapest, Hungary*
Krystell Santamar, *Regional Office for Europe, International Federation of the Red Cross and Red Crescent Societies (IFRC), Budapest, Hungary*

Main findings

- A heat wave in a cold-adapted environment can look quite different from other parts of the world. In Greenland and Iceland infrastructure is built for cold weather, meaning during a heatwave ice melt can lead to flooding and damage roads and infrastructure. In Iceland, bituminous bleeding in the roads created dangerous conditions for drivers. In Greenland, unusual warmth causes sea ice to break up, which threatens communities that depend on it for hunting, fishing, and travel. This affects food security, mobility, scientific research, and Indigenous knowledge. Warmer seas are also shifting fish populations—while cod and mackerel are increasing, cold-water species like shrimp and halibut are moving north, causing economic challenges. Additionally, more seaweed growth and less available fodder have forced farmers to import hay from Iceland, increasing costs and creating cross-border dependencies.
- Temperatures over Iceland as observed this May are record-breaking, more than 13°C hotter than the 1991-2020 average May daily maximum temperatures. In today's climate, which globally has warmed by 1.3°C, the 7-day maximum and temperatures observed in 2025 in the study region have a return time of about once every 100 years. In a 1.3°C colder climate such temperatures would however have been extremely rare.
- When combining the observation-based analysis with climate models, to quantify the role of climate change in this 7-day heat event, we find that climate models underestimate the increase in heat found in observations, but not by as much as in other regions. Based on the combined analysis we conclude that climate change made the extreme heat about 3°C hotter and about 40 times more likely. There is more uncertainty in the estimate for the increase in likelihood and notably it is much smaller than in other heat attribution studies in extratropical latitudes. Given the known underestimation of temperature trends in climate models, this is thus likely an underestimation.
- At a global warming of 2.6°C the likelihood and intensity of such events continue to increase, at least doubling in likelihood and increasing by a further 2°C in intensity.
- The new record of 26.6°C occurred at Egilsstaðir, in East Iceland, and is estimated to have a return period of about 110 years in the current climate. Analysing the Egilsstaðir and Reykjavík stations for Iceland we find slightly lower trends in the magnitude of May maximum 1-day temperatures, compared to the gridded Iceland average 7-day heat. The Ittoqqortoormiit station in East Greenland on the other hand shows a trend in 1-day heat similar to the 7-day Iceland-average heat and extrapolating back to the preindustrial climate indicates that May temperatures have become about 3.9°C hotter since then.
- Both countries reflect the broader Arctic trend for rising temperatures and associated changes in precipitation and hydrology that are beginning to make climate adaptation more pressing. Currently Iceland is in the process of formalising climate change adaptation plans, with necessary improvements to infrastructure and affected societal systems, while Greenland is in the early stages of responding to heat as an emerging public health threat.

1 Introduction

Towards the end of May, much of Greenland and Iceland saw anomalously high temperatures (Fig. 1.1), leading to record-breaking at several locations in Greenland, and a new national May record in

Iceland. These high temperatures were mainly due to a steady flow of warm air from the south, caused by a high-pressure system near the Faroe Islands and a low-pressure system south of Cape Farewell. The temperature at Egilsstaðir Airport, Iceland, reached 26.6°C on May 15, setting a new national record for the month of May. New temperature records were set at 83 Icelandic weather stations, those with at least 20 years in operation, between May 17 and 18. Végeirsstaðir in Fnjóskadalur recorded 26.0°C on May 17, while Húsafell reached 25.7°C on May 18 ([IMO, 2025](#)).

In Greenland, local record-high minimum temperatures have been reached, with Nararsuaq (south Greenland, 61.2°N, 45.4°W) night temperatures not falling below 14.9°C on May 19 ([X, DMI](#)), one of the highest minimums recorded in Greenland. Also Kangerlussuaq, Nuuk and Narsarsuaq saw high daytime temperatures, with both Kangerlussuaq and Narsarsuaq reaching 20°C, which is 11.5°C and 10.1°C above the May 1991-2020 average daily maximum temperatures (TX) respectively (source: DMI). On the colder east side of Greenland, May records were locally broken at Daneborg (12.3°C, 74.3°N, 20.3°W) and at Ittoqqortoormiit (14.3°C, 70.5°N, 22.0°W) by the largest margin (source: DMI). The heat from May 15-21 corresponded with melting of the Greenland ice sheet that was about 17 times higher than average for this time of year, according to preliminary analysis of the Greenland Surface Melt Extent Interactive Chart ([NSIDC, 2025](#)).

While few impacts have been reported at the time of writing, numerous studies demonstrate that such unusually high temperatures early in the year can have significant effects on local ecosystems. These ecosystems, adapted to very cold climates, are sensitive to temperature shifts, and disruptions to their delicate balance can lead to consequences not only for the ecosystems themselves but also for the communities that depend on them.

In addition, the heat also directly affects communities adapted to cold climates. Iceland and Greenland are quite different when it comes to development and access to basic services, and the strength of their infrastructure greatly affects how communities can deal with heat. In Greenland, especially in rural and remote areas, coping with heat is quite challenging. For example, during the extreme heat and heavy rain in 2022, melting permafrost caused iron and other metals to enter many Arctic lakes, raising concerns about water quality and environmental impacts. Sanitation is also less developed: while urban areas have piped sewage systems, about 90% of rural homes use bag toilets that are dumped in open areas, increasing health risks, especially in warmer weather when bacteria grow faster ([Hendriksen & Hoffman, 2017](#)).

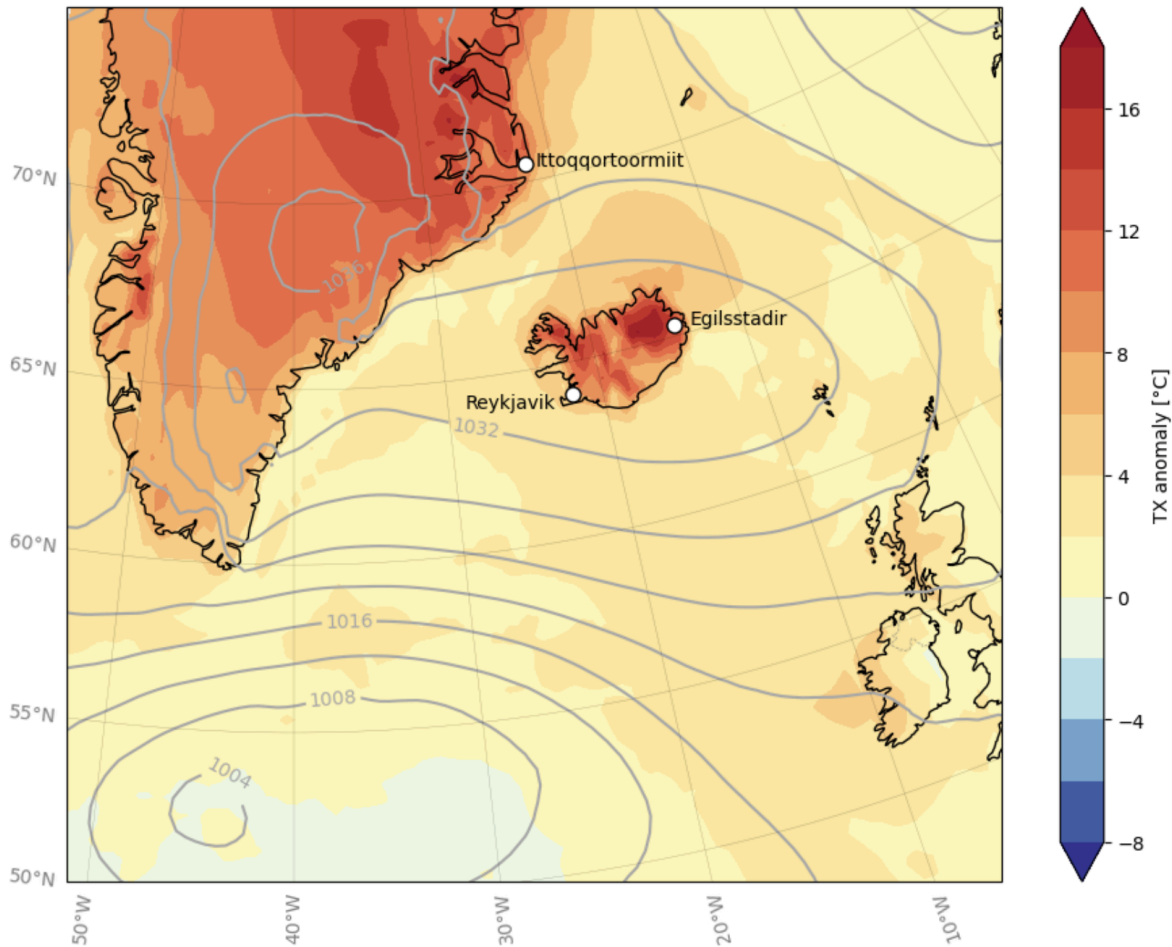


Figure 1.1: Anomaly in daily maximum temperature (TX) on 19 May 2025 (date of record breaking at Ittoqqortoormiit), with respect to the May mean TX 1991-2020 climatology [$^{\circ}\text{C}$] (shading) and mean sea level pressure [hPa] (grey contours), and locations of stations used in the study. Source: ERA5.

An anticyclonic block had developed over the North Atlantic around 14 May with a region of high pressure over Iceland and lows northeast of Newfoundland and Poland (Fig. 1.2). During the blocking period, a pool of very warm air moved further northwest to Greenland, where a high formed over the ice sheet between Tasiilaq and Ittoqqortoormiit. This meant that the originally very warm air was blown downhill on the stretch from Danmarkshavn to Ittoqqortoormiit, rendering much of Greenland under the influence of the very warm pool of Iberian descent. From around May 21st the meteorological situation was closer to a normal situation for Greenland, with a low pressure system near Iceland and temperatures returning to more average May temperatures. The southerly flow driven by the anticyclone as well as low-pressures south of Cape Farewell also resulted in record temperatures in Iceland. This pattern lasted for approximately nine days, leading to high temperatures across the region. While similar weather patterns have occurred in the past (see also Section 3.3 for historical analogues of this circulation pattern), this heatwave was exceptional for its early timing and prolonged duration.

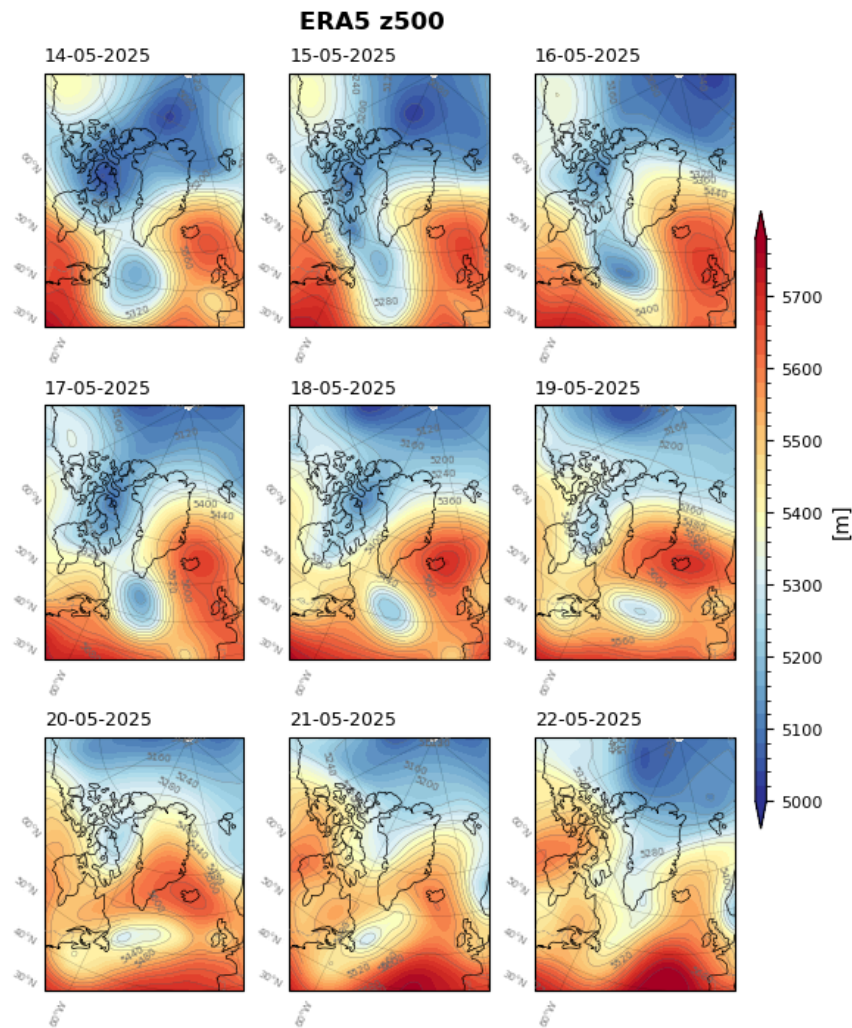


Figure 1.2: Geopotential height at 500hPa during the period of the event. Data: ERA5.

1.1 Review of trend and attribution studies on extreme heat events for the region

Surface temperatures in the Arctic have in recent decades increased at more than double the global average, a phenomena recognized as the Arctic Amplification ([Meredith et al., 2022](#) (Box 3)). While the mechanisms responsible are still debated ([Li et al., 2024](#)), reductions in both sea ice and snow cover have also taken place as have extremes in temperature ([Overland, and Wang, 2018a](#); [Overland and Wang 2018b](#)).

Human-induced climate change has increased the frequency and severity of extreme heat events globally, with adverse impacts on human health, livelihoods and infrastructure, particularly in urban areas ([IPCC 2023](#)). Over the past half century, Greenland and Iceland have experienced an increase in both the intensity and frequency of extreme high temperature events, a trend that is projected to continue into the future ([Seneviratne, et. al, 2021](#)).

Sea ice extent in the Arctic has declined substantially in the satellite era and in recent years the minimum extent has been about ~50% of the values typical for the 1980s ([Meier et al., 2024](#)). Whilst the 2025 May heat could be linked to an increased melting of the Greenland ice sheet, sea ice extent east of Greenland has not diminished much and during the month of May, the extent was close to normal for the 1981 - 2010 reference period ([NSIDC 3 June 2025](#), Fig. 1b).

1.2 Event Definition

Iceland (Fig. 1.3a) and Greenland temperatures peak over the summer months June-August. Iceland experienced exceptionally warm weather from May 13 to 22, 2025, with temperatures significantly above the month average (Fig. 1.3a). The most pronounced maximum temperature (TX) anomalies occurred in the northeastern and eastern highlands, where the 7-day average anomaly exceeded 13°C (Fig. 1.3c). The most significant record-breaking heatwaves in recent years occurred around the end of July and beginning of August 2008, and in August 2004, with temperatures in excess of 20°C for several days in a row ([IMO, 2025](#)). Occurring later in the season, the 2004 and 2008 heatwaves reached even higher temperatures than the 2025 May event, however the 2025 May event was the most anomalous with respect to the maximum temperatures expected for the time of year. This heat event was exceptional for its duration but also broke records on the daily time scale. We therefore choose to analyse two timescales and two spatial scales: 7-days, to represent the long duration at high anomalous amplitude over a large area, and 1-day, to examine exceptional heat days on local scales. As we are interested in understanding the trends in similar early season heatwaves, we focus the analysis on the month of May only. We chose to focus on Iceland as the domain for the large-scale attribution analysis, as the heat was particularly long-lasting there and more people were affected, whereas in Greenland the centre of anomalous heat moved regionally through May. The thin coastal areas that experienced high temperatures in Greenland are also more challenging for models to represent. For the small scale 1-day extremes we examine observations only, selecting one station in Greenland and two in Iceland. The Greenland station of Ittoqqortoormiit is selected as it provides a long time series of TXx in a region that experienced extreme heat. For Iceland, Egilsstaðir Airport is chosen as the location of the national record in a region of extreme heat, and additionally the station Reykjavik, which provides a longer and consistent time series for comparison. The event definition for the remainder of this article is (i) the maximum 7-day Iceland-averaged TX (maximum temperature) in May (each year, the maximum of 31 overlapping 7-day periods is selected, where the first 7-day period considered is 28 April to 4 May, centered on 1 May, and the last 7-day period considered is 28 May to 3 June, centered on 31 May), referred to here as TX7x-May, and (ii) the observed May maximum of single day maximum temperatures at an individual station, referred to here as TXx-May.

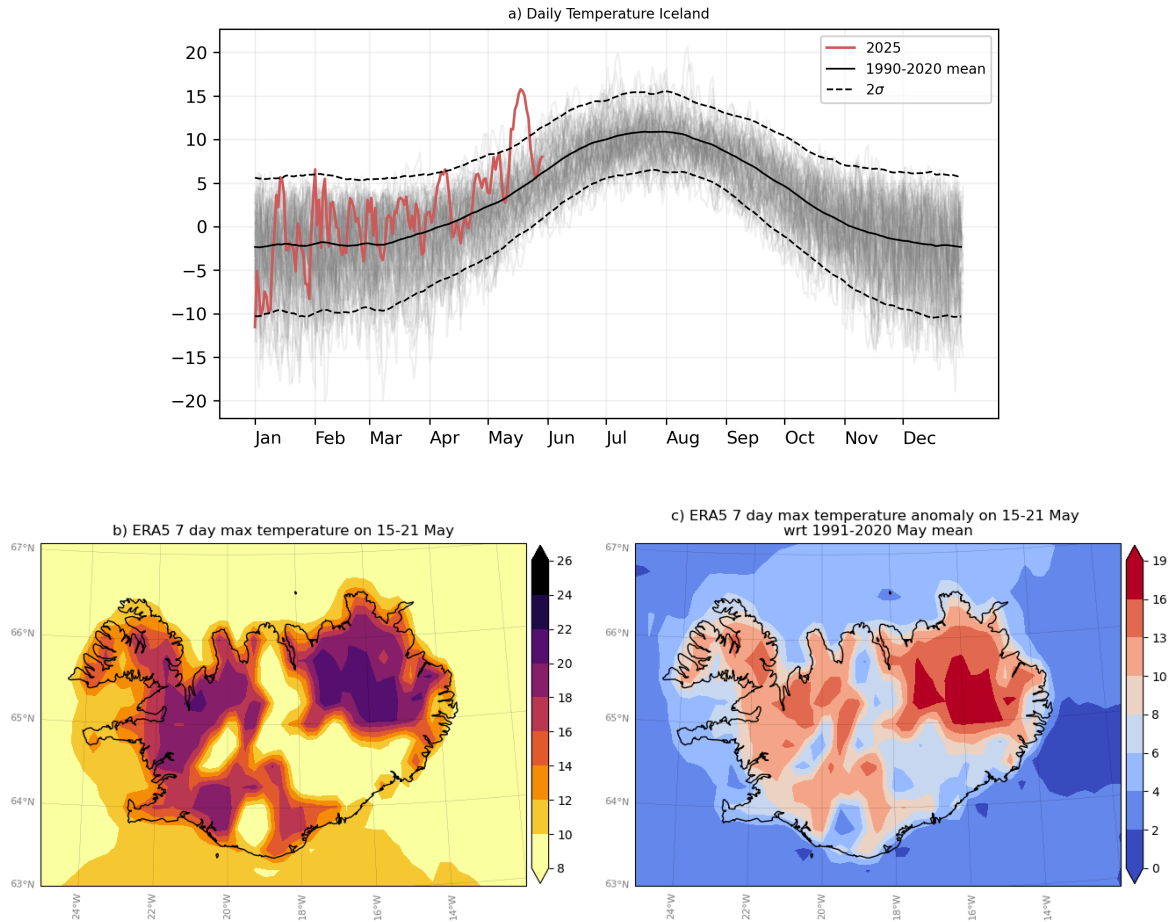


Figure 1.3: Daily variability of maximum temperature over the study region (a), seven day average maximum temperature ($TX7x$) for the period of 15 of May to 21 May (b) and $TX7x$ anomaly with respect to May climatology over the period of 1991-2020. Data ERA5.

In this report, we study the influence of anthropogenic climate change by comparing the likelihood and intensity of similar $TX7x$ -May extremes at present with those in a 1.3 °C cooler climate. We also extend this analysis into the future by assessing the influence of a further 1.3 °C of global warming from present. This is in line with the latest Emissions Gap Report from the United Nations Environment Programme, which shows that the world is on track for at least 2.6 °C temperature rise given currently implemented policies ([UNEP, 2024](#)).

2 Data and methods

2.1 Observational data

We first use observational and reanalysis data to estimate the return period of a similar $TX7x$ -May event in the present day and to assess the historical trends with increasing GMST. The datasets used are as follows:

The European Centre for Medium-Range Weather Forecasts's 5th generation reanalysis product, ERA5, is a gridded dataset that combines historical observations into global estimates using advanced modelling and data assimilation systems ([Hersbach et al., 2020](#)). We use daily maximum temperatures data from this product at a resolution of $0.25^{\circ} \times 0.25^{\circ}$, from the years 1950 to present. The re-analysis is available until the end of the preceding month (April 2025). We extend the re-analysis data with the ECMWF analysis (for 1 to 21 May) to cover the period of the event.

We use CPC daily maximum temperature. This is the gridded product from NOAA PSL, Boulder, Colorado, USA known as the CPC Global Unified Daily Gridded data, available at $0.5^{\circ} \times 0.5^{\circ}$ resolution, for the period 1979-present. Data are available from [NOAA](#).

As a third gridded dataset we use the Copernicus Arctic Regional ReAnalysis (CARRA) dataset, a state of the art data-driven reanalysis from the Copernicus Climate Change Service (C3S). It is updated on a monthly basis, with data available from September 1990 to March 2025, and thus currently excludes the 2025 event. The CARRA-West domain is used here, which centers on Greenland and also covers Iceland. CARRA uses global ERA5 reanalysis as boundary forcing and has a $2.5 \text{ km} \times 2.5 \text{ km}$ grid, providing more local detail than the coarser resolution products of the ERA5 global reanalysis. Whilst CARRA is considered to be the best gridded dataset for the study of Greenland and Iceland, it is shorter than ERA5 and CPC and does not contain the 2025 event. It is used here to verify the order of magnitude of ERA5 and CPC results, which are subsequently used in the synthesis. Data are available from the [C3S](#) Climate Data Store.

To assess the peak extremity of the event from a local perspective, we analyse May TXx from station data. We use one synoptic station series from Greenland – Ittoqqortoormiit (70.45°N , 22.0°W), provided by the Danish Meteorological Institute, and two synoptic station series from Iceland – Reykjavik (64.1°N , 21.9°W) and Egilsstaðir Airport (65.3°N , 14.4°W), provided by the Icelandic Met Office (See Fig. 1.1 for station locations).

The Ittoqqortoormiit time series is constructed from two stations (4340 and 4339-Ittoqqortoormiit), separated by 8 km (which is the standard practice of the Danish Meteorological Institute (DMI) in their climate monitoring of daily mean temperature). The combined series of daily maximum temperatures has been quality checked by DMI but is neither gap-filled nor homogenised. The Egilsstaðir Airport series used in this study is made by combining the manual station data, from 1955 to 1997, with the digital station data, from 1998 to present, on the same premises.

As a measure of anthropogenic climate change we use the (low-pass filtered) global mean surface temperature (GMST), where GMST is taken from the National Aeronautics and Space Administration (NASA) Goddard Institute for Space Science (GISS) surface temperature analysis (GISTEMP, [Hansen et al., 2010](#) and [Lenssen et al., 2019](#)).

2.2 Model and experiment descriptions

We use multi-model ensembles from climate modelling experiments using very different framings ([Philip et al., 2020](#)): Coupled Global Circulation Models and Sea Surface temperature (SST) driven global circulation high resolution models.

CMIP6: This coupled GCM ensemble consists of simulations from 18 participating models with varying resolutions. For more details on CMIP6, please see [Eyring et al., \(2016\)](#). For all simulations, the period 1850 to 2015 is based on historical simulations, while the SSP5-8.5 scenario is used for the remainder of the 21st century. Note that, as we evaluate projections at a warming level (+2.6°C) rather than specific years, the results will not be very sensitive to the choice of scenario.

HighResMIP: This is an SST-forced model ensemble ([Haarsma et al. 2016](#)), the simulations for which span from 1950 to 2050. The SST and sea ice forcings for the period 1950-2014 are obtained from the 0.25° x 0.25° Hadley Centre Global Sea Ice and Sea Surface Temperature dataset that have undergone area-weighted regridding to match the climate model resolution. For the ‘future’ time period (2015-2050), SST/sea-ice data are derived from RCP8.5 (CMIP5) data, and combined with greenhouse gas forcings from SSP5-8.5 (CMIP6) simulations (see Section 3.3 of Haarsma et al. 2016 for further details).

2.3 Statistical methods

Methods for observational and model analysis and for model evaluation and synthesis are used according to the World Weather Attribution Protocol, described in [Philip et al., \(2020\)](#), with supporting details found in [van Oldenborgh et al., \(2021\)](#), [Ciavarella et al., \(2021\)](#), [Otto et al., \(2024\)](#) and [here](#). The key steps, presented in sections 3-6, are: (3) trend estimation from observations; (4) model validation; (5) multi-method multi-model attribution; and (6) synthesis of the attribution statement.

In this report we analyse time series of TX7x-May over Iceland, and TXx-May for one station in Greenland and two stations in Iceland.

A nonstationary GEV distribution is used to model TX7x-May and TXx-May and the distribution is assumed to shift linearly with GMST, while the variance remains constant. The parameters of the statistical model are estimated using the principle of maximum likelihood.

For each time series we calculate the return period and intensity of the event under study for the 2024 GMST and for 1.3 C cooler GMST: this allows us to compare the climate of now and of the preindustrial past (1850-1900, based on the [Global Warming Index](#)), by calculating the probability ratio (PR; the factor-change in the event's probability) and change in intensity of the event.

3 Observational analysis: return period and trend

3.1 Analysis of gridded data

The GEV distribution fits the gridded datasets quite well. Using ERA5 (re)analysis data the TX7x-May event over Iceland has a magnitude of 14.7 °C. Locally, recorded temperatures were much higher. Using ERA5 data from 1950 onwards and a GEV that shifts with the smoothed GMST, we calculate for May TX7x the return period in the current climate, change in intensity and probability ratio between the 2025 climate and a past climate that is 1.3 °C cooler than now (i.e. without

anthropogenic warming), see Fig. 3.1. The return period is estimated to be about 400 years (95% CI 50 to infinity). Using CPC TX7x-May data from 1979 onwards, we repeat the same analysis. The TX7x-May event over Iceland has a magnitude of 16.6 °C in this dataset. The return period in the current climate is estimated to be about 70 years (95% CI 14 to infinity). For the model analysis we use a rounded return period of 100 years to characterise the event. Using CARRA TX7x-May data from 1991 to 2024 we repeat the analysis but in this case, as the data does not yet extend as far as 2025, we cannot evaluate the magnitude or return period of the event in this dataset. Instead, we evaluate the changes between the past and present climate for an event of a 100 year return period in the year 2025.

The change in intensity is 4.95°C (95% CI 3.04 to 7.13°C) in ERA5 and 3.92°C (95% CI -1.83 to 6.54°C) in CPC. The wider uncertainty range in the CPC dataset compared to the ERA5 dataset is due to the shorter coverage of the CPC dataset. The relatively large uncertainty margins are a result of the relatively large variability of May maximum temperatures over Iceland. For ERA5 we can only estimate a lower bound of the Probability Ratio of 22706. This is due to the combination of the strong trend and the large return period in the time series. As both the trend and the return period in the CPC dataset are slightly lower, we can estimate both the best estimate and the lower bound of the Probability Ratio: 4716 (>5.542). Results for CARRA agree with the CPC and ERA5 results, although the Probability Ratio is not very reliable due to the assumption on the magnitude of the event combined with a more negative GEV shape parameter – the tail of the distribution converges faster to an upper limit in TX7x – which may be related to larger uncertainties in the shape of the fit due to a shorter dataset. Also, the best estimate of the intensity change is slightly lower, however, the lower bound is higher than that of CPC while the upper bound is more or less the same. Due to the assumption on the magnitude and the larger uncertainties that arise from the short length of the dataset we do not include the CARRA trends in the synthesis analysis.

Table 3.1: *Estimated return periods of TX7x-May over Iceland in the reanalysis and observational datasets with coverage of the event. The CARRA dataset does not include data for the event. The event magnitude given in the table corresponds to the magnitude that an event would have with a return period of 100 years in the year 2025.*

Dataset	Magnitude (°C)	Return period (95% C.I.)	Probability ratio (95% CI)	Intensity change (°C) (95% CI)
ERA5	14.652	443.5 (>50.053)	>22706	4.956 (3.041 to 7.13)
CPC	16.627	70.356 (>13.963)	4716.5 (>5.5418)	3.922 (-1.83 to 6.536)
CARRA	NA (11.870)	100	> 6.1715	2.699 (-1.018 to 6.648)

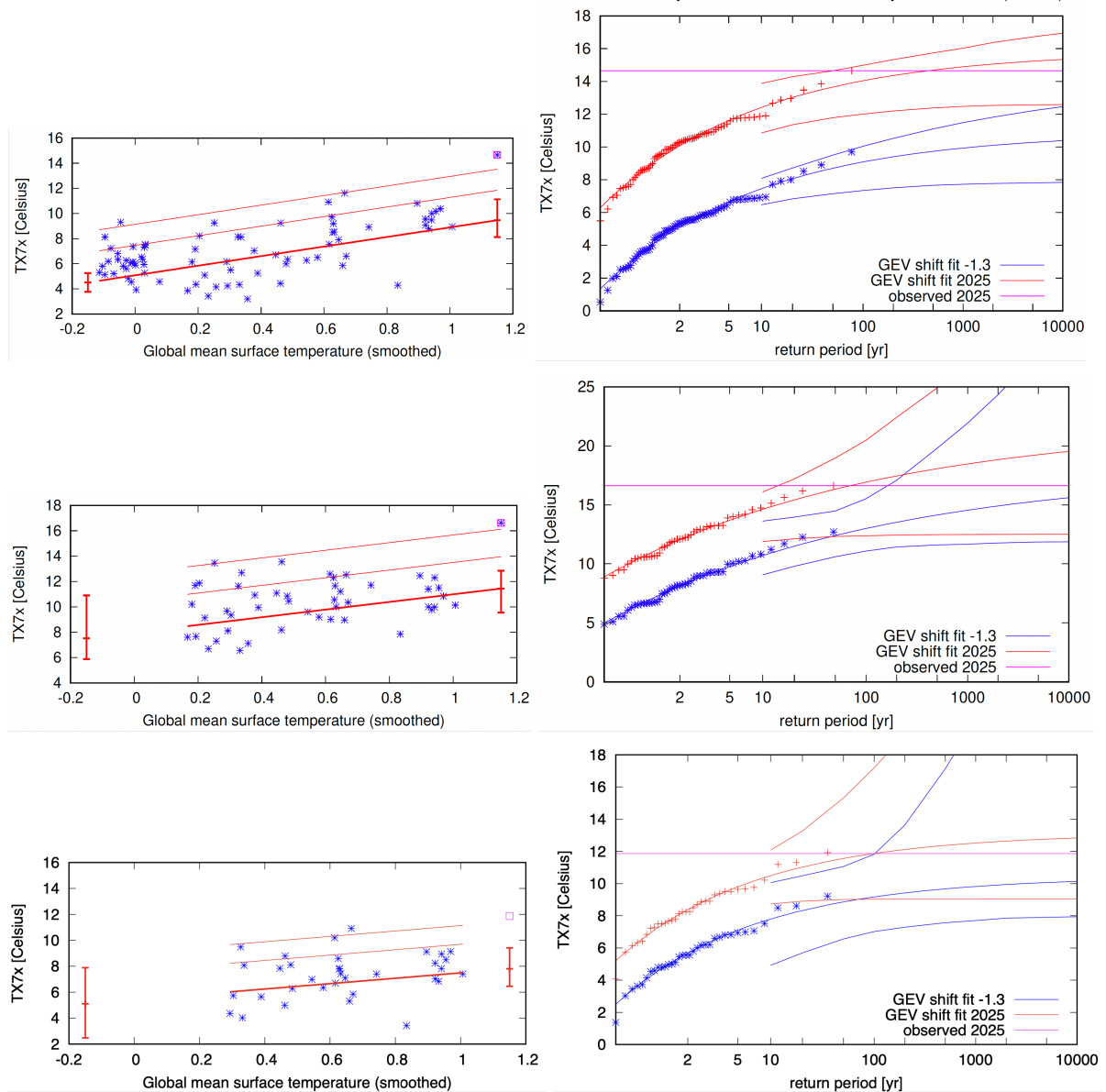


Figure 3.1. Left: $TX7x$ -May over Iceland estimated from gridded data to change in global mean temperature. The thick red line denotes the time-varying mean, and the thin red lines show 1 standard deviation ($s.d$) and 2 $s.d$ above. The vertical red lines show the 95% confidence interval for the location parameter, for the current, 2025 climate and the hypothetical, 1.3°C cooler climate. The May 2025 observation is highlighted with the magenta box. Right: Return periods for the 2025 climate (red lines) and the 1.3°C cooler climate (blue lines with 95% CI). The top figures are based on ERA5 data, the central figures on CPC data and the bottom figures on CARRA data..

3.2 Analysis of synoptic station (point) data

As for the gridded observational data, the station data time series (Fig. 3.2) are fitted with a GEV that shifts with smoothed GMST (Fig 3.3), and then the return period in the current climate, the change in intensity and the Probability Ratio – between the past 1.3°C cooler climate and now – are calculated. Results are summarised in Table 3.2.

Table 3.2: Estimated return periods, probability ratios and intensity changes of TXx-May for the three synoptic station time series.

Station	Magnitude [°C]	Return period (95% C.I.)	Probability ratio (95% CI)	Intensity change [°C] (95% CI)
Ittoqqortoormiit	14.3°C (19 May)	57.435 (>14.653)	110.46 (>6.0162)	3.867 (1.615 to 6.393)
Egilsstaðir Airport	26.6°C (15 May)	148.44 (>22.241)	Inf (>0.69)	2.475 (-0.736 to 5.304)
Reykjavik	20.2°C (16 May)	46.548 (17.466 to 48327)	4.731 (>1.0186)	1.514 (0.008 to 3.182)

The Ittoqqortoormiit time series combines data from station 4340 (from 1958) with station 4339 (from 1981). The TXx-May 2025 event (19 May 2025) had a magnitude of 14.3°C, which in the current climate has a return period of about 60 years (95% CI 14.7 to infinity). The change in intensity between the past 1.3°C cooler climate and now is 3.9°C (95% CI 1.6°C to 6.4°C), and the corresponding change in Probability Ratio is about 110 (95% CI 6.0 to infinity). To test the robustness of the results on the combination of the two station series, we also analyse the data from 1981 onwards (that is, station 4339 only) separately. The change in intensity is still the same order of magnitude, at 3.5 °C (95% CI -0.2 to 8.6), while the PR is an order lower at 13.3 (0.9 to infinity) and the return period is estimated at around 50 years, with each of these metrics showing increased uncertainty due to the shorter time series.

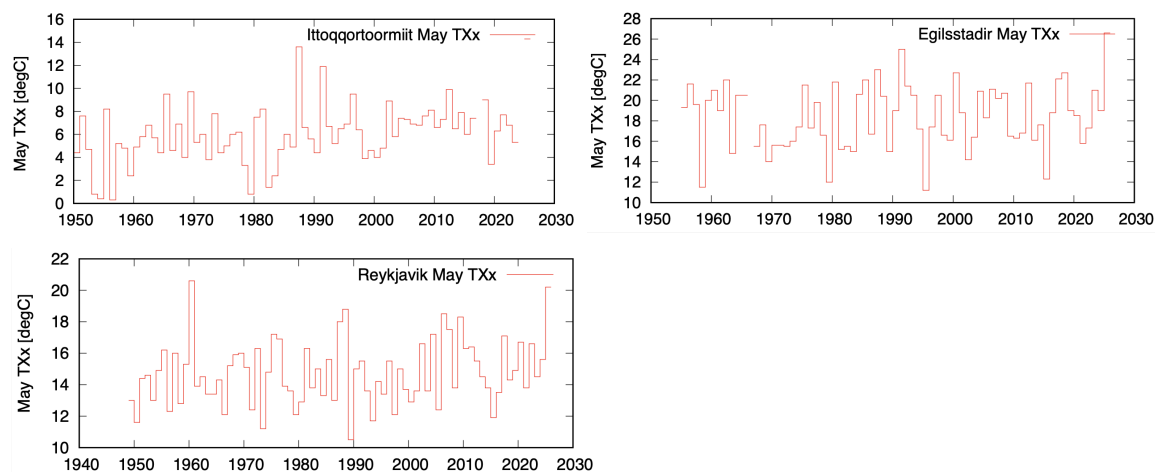


Figure 3.2: Time series of May TXx of station data from (a) Ittoqqortoormiit, Greenland, (b) Egilsstaðir Airport, Iceland, and (c) Reykjavik, Iceland.

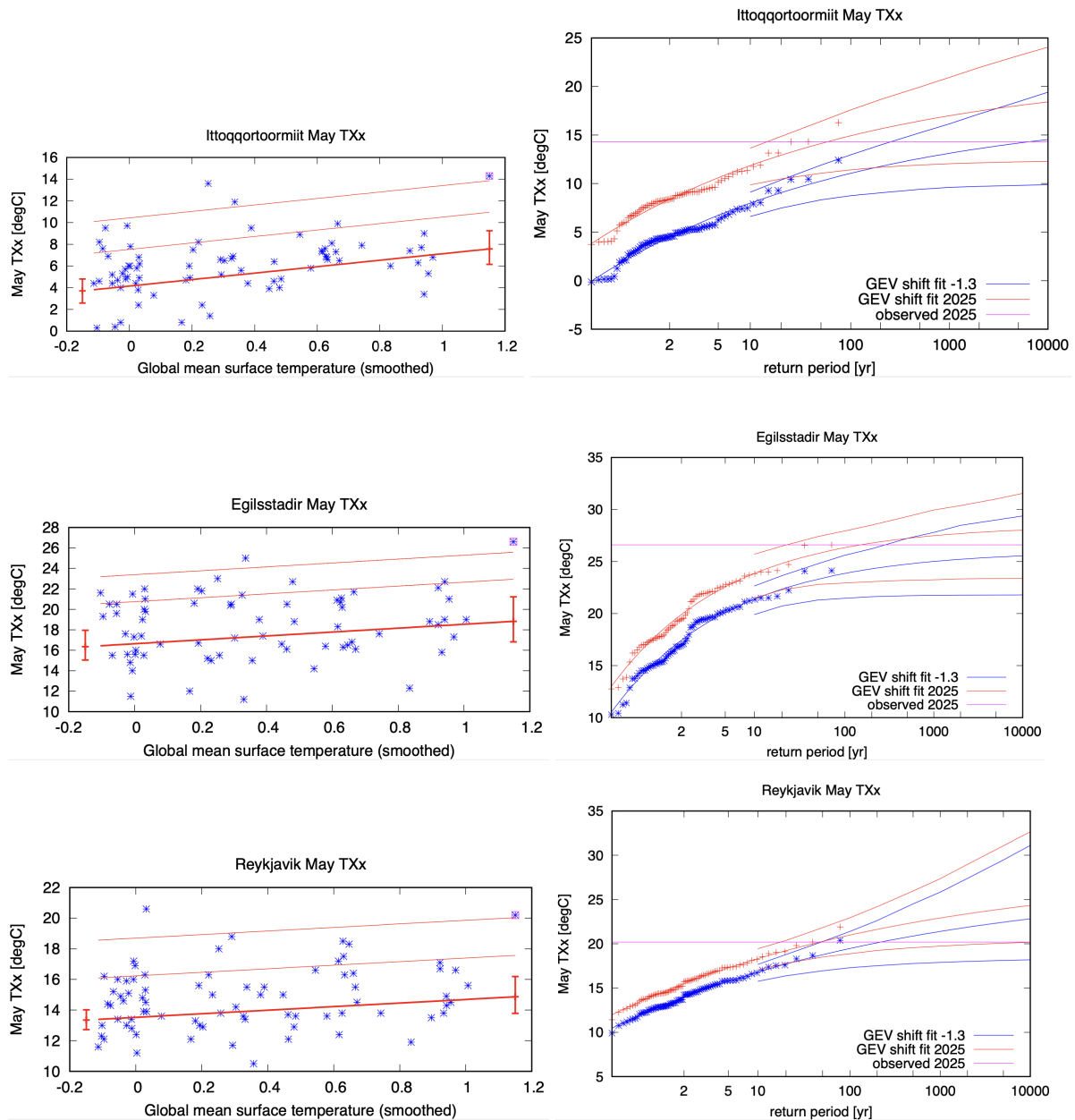


Figure 3.3: Analysis of synoptic station data from (a) Ittoqqortoormiit, Greenland, (b) Egilsstaðir, Iceland, and (c) Reykjavik, Iceland. Left panels: May TXx with respect to change in global mean temperature. The thick red line denotes the time-varying mean, and the thin red lines show 1 standard deviation (s.d) and 2 s.d above. The vertical red lines show the 95% confidence interval for the location parameter, for the current, 2025 climate and the hypothetical, 1.3°C cooler climate. The May 2025 observation is highlighted with the magenta box. Right panels: Return periods for the 2025 climate (red lines) and the 1.3°C cooler climate (blue lines with 95% CI).

At Egilsstaðir Airport, the Icelandic May temperature record was broken, with Tmax reaching 26.6°C on 15 May 2025. The return period of an event of that magnitude at this station location is estimated at about 150 years (95% CI 22.2 to infinity). The change in intensity in May TXx events between the 1.3°C cooler past and the present climate is estimated to be about 2.5°C (95%CI -0.7 to 5.3). The best

estimate for the return period in the past climate is much greater than 10'000 years and as such the probability ratio is undefined. If the 2025 event is excluded from the analysis (not shown), the fitted trend is somewhat less positive, with a change in intensity of about 1.0°C, but still with an undefined probability ratio, due to the negative shape parameter of the distribution and the extreme event magnitude. As this station series contains a switch from manual to automatic recording, we examine an additional station series for Iceland - Reykjavik - as this is a long series from one station location that is manned.

At Reykjavik, the May maximum temperature reached 20.2°C on 16 May 2025. The return period of such an event is about 47 years in the current climate. The change in intensity between the past and the present climate is estimated at 1.5°C (95% CI 0.01 to 3.2°C) and the probability ratio at 4.7 (1.0 to infinity). This trend is slightly lower than in the other stations.

The trends in station data 1-day May maximum temperatures are slightly lower than in the gridded datasets, which may be due to the difference between point data and gridded data, as well as the averaging of the gridded data over all of Iceland and the quality of the gridded data. We checked that a similar analysis of station data but for TX7x-May instead of TXx-May does not change this result significantly.

3.3 Circulation analogues

Atmospheric flow analogues can be used to assess changes in the intensity of dynamically similar events or changes in the frequency of occurrence of particular circulation patterns ([Vautard et al., 2023](#); [Jézéquel et al., 2018](#)). Here we use ERA5 data to assess so-called analogues identified from 500 hPa geopotential height (Z500) since 1950, to detect trends in the frequency of circulation patterns similar to the omega-pattern associated with the heatwave.

To identify the most similar events, we compute the Euclidean distance between the Z500 anomaly field of the 17th May 2025 and every other day (months March-May, 1950–2024) over the region bounded by [40° to 0°W, 40° to 80°N]. To avoid double-counting persistent events, the identified events must be separated by at least 5 days. The analogues are determined over a specific domain and using Z500. These were chosen by assessing the event itself, and current understanding of the circulation drivers of similar events. Other events with similar extreme temperatures are associated southerly flow patterns, with low pressure over the North Atlantic and high pressure over Iceland. The domain was chosen to cover these key features.

To detect trends in the circulation pattern and intensity since 1950 we identify the closest 29 analogues across the two periods (1950-1980 and 1994-2024). This corresponds to the closest 1% of days in each period. The average weather conditions associated with the two sets of analogues - called 'composites' - are then compared to assess differences between the two periods. We also assess the change in frequency of the closest analogues through time. This is assessed at three different thresholds - the upper 5% of days, upper 10%, and upper 20%. Differences in modes of internal variability between the two time periods can also induce differences in the weather conditions,

therefore we cannot identify the role of climate change solely by comparing analogue sets in reanalyses.

We can assess the difference in the fields of composites, for both the analogue circulation variable (Z500) and meteorological hazards (temperature). Fig. 3.4 a-c shows that the analogues look qualitatively good with similar circulation patterns as in the composites for both periods. The present day analogues are weaker over both the regions with low and high pressure, however the change is only significant over the southwest corner of the domain. The compositions of the temperature analogues show that they are significantly warmer in the present day period, particularly over Iceland (Fig. 3.4 f-h). This is likely the thermodynamic contribution.

We also assess the change in annual frequency of the most similar events (Fig. 3.5). For all three thresholds there is a significant negative trend through time. This means that similar circulation patterns are becoming less frequent and/or less persistent.

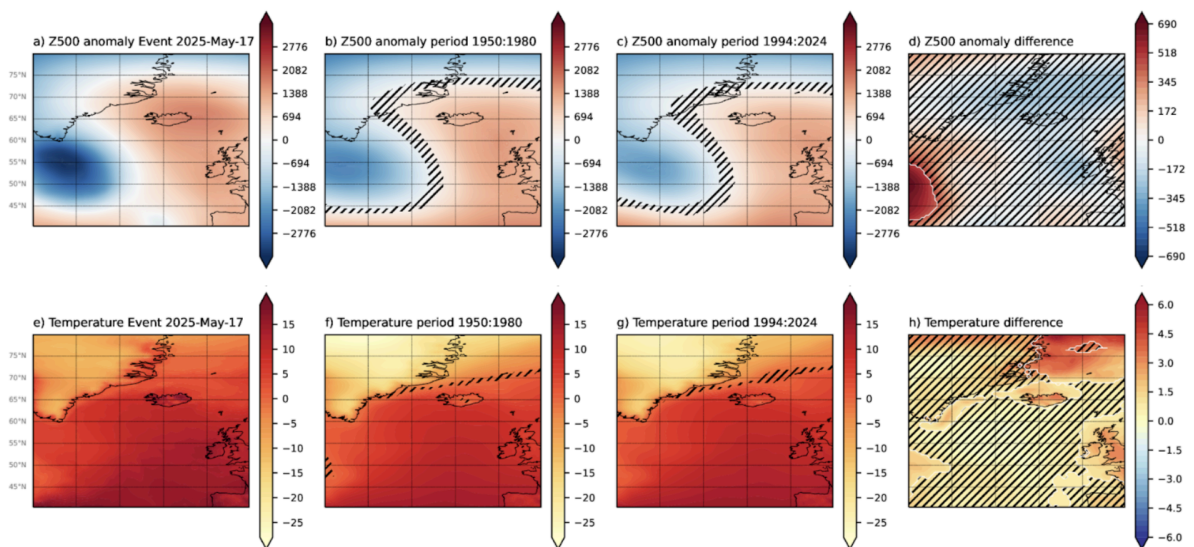


Figure 3.4: Changes in atmospheric analogues. (a) Z500 for the event, 17th May 2025. (b) Composite of the top 30 analogue days from the past period, 1950-1980. (c) Composite of the top 30 analogue days from the present period, 1994-2024. (d) Difference between the composites of past and present (present minus past). (e-h) as in a-d for the 2m temperature field (°C). Z500 used to identify analogues in all plots. Hashing signifies regions where the signal is not significant based on a two-sided t-test.

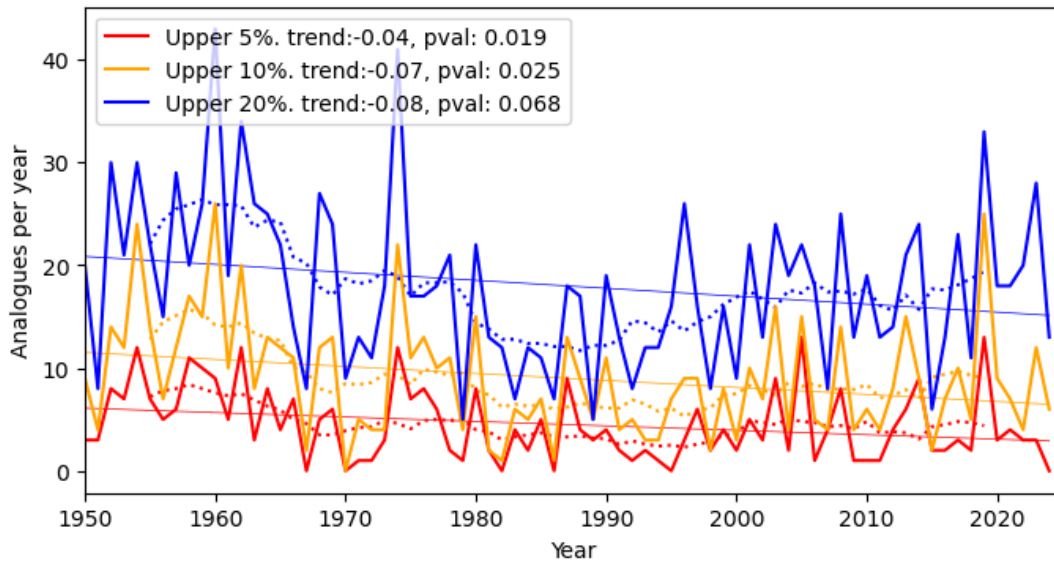


Figure 3.5: Trends in frequency of the most similar events. Number of “good” analogues per year (in MAM) at three threshold levels: the closest 5%, 10% and 20% of most similar days (based on Euclidean distance of Z500 field). Multiannual trends (dotted lines) are plotted.

4 Model evaluation

In the subsections below we show the results of the model evaluation for each location. The climate models are evaluated against the observations in their ability to capture:

1. Seasonal cycles: For this, we qualitatively compare the seasonal cycles based on model outputs against observations-based cycles. We discard the models that exhibit ill-defined peaks in their seasonal cycles. We also discard the model if the warm season onset/termination varies significantly from the observations.
2. Spatial patterns: Models that do not match the observations in terms of the large-scale May average Tmax patterns are excluded. Models are labeled 'good' if they have a minimum inside Iceland, reasonable if they show some minimum towards the inland, and 'bad' if they do not show a minimum over Iceland at all.
3. Parameters of the fitted statistical models. We discard the model if the model and observation parameters ranges do not overlap.

The models are labelled as ‘good’, ‘reasonable’, or ‘bad’ based on their performances in terms of the three criteria discussed above. A model is given an overall rating of ‘good’ if it is rated ‘good’ for all three characteristics. If there is at least one ‘reasonable’, then its overall rating will be ‘reasonable’ and ‘bad’ if there is at least one ‘bad’. We use models that are labeled 'good' and models that have at most one label 'reasonable', see column 'Conclusion' in Table 4.1. One exception to this is the model ACCESS-ESM1-5, which has undefined best estimates as well as undefined lower and upper bounds for projected probability ratios. To keep the same models in the past and projected analysis periods, this model is omitted from the synthesis.

Table 4.1 Evaluation results of the climate models considered for attribution analysis of TX7x-May. For each model, the threshold for a 1-in-100-year event is shown, along with the best estimates of the Sigma and Shape parameters are shown, along with 95% confidence intervals. Furthermore evaluation of the seasonal cycle and spatial pattern are shown.

Model / Observations	Seasonal cycle	Spatial pattern	Sigma	Shape parameter	Conclusion
ERA5			1.75 (1.43 ... 2.09)	-0.28 (-0.52 ... -0.16)	
CPC			1.69 (1.24 ... 2.16)	-0.16 (-0.78 ... 0.14)	
ACCESS-CM2	good	reasonable	1.91 (1.53 ... 2.26)	-0.13 (-0.37 ... 0.040)	1x reasonable
ACCESS-ESM1-5	good	reasonable	1.62 (1.32 ... 1.91)	-0.37 (-0.58 ... -0.20)	1x reasonable (eliminated)
CanESM5	reasonable	bad	1.60 (1.30 ... 2.00)	-0.41 (-0.87 ... -0.25)	bad
CMCC-ESM2	good	reasonable	1.87 (1.46 ... 2.24)	-0.22 (-0.39 ... -0.070)	1x reasonable
CNRM-CM6-1-HR	reasonable	good	1.54 (1.18 ... 1.85)	-0.10 (-0.32 ... 0.15)	1x reasonable
CNRM-CM6-1	good	good	1.56 (1.27 ... 1.77)	-0.25 (-0.45 ... -0.090)	good
EC-Earth3	good	good	1.52 (1.20 ... 1.76)	-0.19 (-0.31 ... -0.020)	good
EC-Earth3-Veg	good	good	1.37 (1.11 ... 1.58)	-0.28 (-0.46 ... -0.090)	good
EC-Earth3-Veg-LR	good	reasonable	2.35 (1.71 ... 2.82)	-0.34 (-0.53 ... -0.060)	2x reasonable
FGOALS-g3	bad	bad	1.70 (1.27 ... 1.98)	-0.13 (-0.44 ... 0.020)	bad
INM-CM4-8	good	good	1.62 (1.35 ... 1.86)	-0.27 (-0.46 ... -0.15)	good
INM-CM5-0	good	good	1.43 (1.14 ... 1.68)	-0.25 (-0.55 ... -0.11)	good
IPSL-CM6A-LR	good	good	1.35 (1.07 ... 1.60)	-0.38 (-0.56 ... -0.20)	good
MIROC6	bad	bad	1.97 (1.55 ... 2.28)	-0.22 (-0.40 ... -0.070)	bad
MPI-ESM1-2-HR	good	good	1.18 (0.960 ... 1.37)	-0.19 (-0.38 ... -0.060)	1x reasonable
MPI-ESM1-2-LR	bad	good	0.940 (0.690 ... 1.10)	-0.15 (-0.32 ... 0.030)	bad
MRI-ESM2-0	good	reasonable	2.37 (1.96 ... 2.91)	-0.58 (-1.0 ... -0.40)	2x reasonable
NorESM2-MM	good	reasonable	1.37 (1.02 ... 1.58)	-0.21 (-0.35 ... 0.050)	1x reasonable
CNRM-CM6-1_r1i1p1f2	good	good	1.34 (1.11 ... 1.53)	-0.021 (-0.18 ... 0.18)	good
CNRM-CM6-1-HR_r1i1p1f2	good	good	1.34 (1.07 ... 1.55)	-0.18 (-0.60 ... -0.094)	good
EC-Earth3P_r1i1p1f1	good	good	1.31 (1.06 ... 1.49)	-0.15 (-0.31 ... -0.0094)	good
EC-Earth3P-HR_r1i1p1f1	good	good	1.37 (1.14 ... 1.57)	-0.27 (-0.40 ... -0.15)	good
HadGEM3-GC31-HM_r1i1p1f1	good	good	1.44 (1.14 ... 1.68)	-0.19 (-0.36 ... -0.033)	good

HadGEM3-GC31-LM_r1i14p1f1	good	good	1.81 (1.38 ... 2.12)	-0.17 (-0.38 ... 0.024)	good
HadGEM3-GC31-M_r1i1p1f1	good	good	1.00 (0.812 ... 1.16)	-0.035 (-0.15 ... 0.11)	bad
MPI-ESM1-2-HR_r1i1p1f1	good	good	1.36 (1.09 ... 1.57)	-0.20 (-0.61 ... -0.082)	good
MPI-ESM1-2-XR_r1i1p1f1	good	good	1.48 (1.17 ... 1.76)	-0.37 (-0.55 ... -0.19)	good

5 Multi-method multi-model attribution

This section shows Probability Ratios and change in intensity ΔI for models that passed model evaluation and also includes the values calculated from the fits with observations.

Table 5.1. Event magnitude, probability ratio and change in intensity for 100-year return period for TX7x-May for observational datasets and each model that passed the evaluation tests. (a) from pre-industrial climate to the present and (b) from the present to 2.6°C above pre-industrial climate.

Model / Observations	Threshold for return period 100 yr	Current warming level [1.3 °C]		Future warming level [2.6 °C]	
		Probability ratio PR [-]	Change in intensity ΔI [°C]	Probability ratio PR [-]	Change in intensity ΔI [°C]
ERA5	14.652 °C	∞ (2.3e+4 ... ∞)	5.0 (3.0 ... 7.1)		
CPC	16.627 °C	4.7e+3 (5.5 ... ∞)	3.9 (-1.8 ... 6.5)		
	°C	(...)	(...)		
ACCESS-CM2	11 °C	5.1 (1.2 ... ∞)	1.6 (0.24 ... 3.7)	7.1 (3.8 ... 67)	2.0 (1.6 ... 2.5)
ACCESS-ESM1-5	13 °C	∞ (∞ ... ∞)	4.0 (2.9 ... 5.0)	25 (11 ... 5.0e+2)	2.4 (1.9 ... 3.0)
CMCC-ESM2	11 °C	1.4 (0.029 ... 21)	0.24 (-1.6 ... 1.8)	1.8 (1.1 ... 4.5)	0.65 (0.050 ... 1.2)
CNRM-CM6-1-HR	11 °C	10 (1.9 ... ∞)	2.0 (0.50 ... 3.6)	8.8 (4.4 ... 67)	1.9 (1.4 ... 2.3)
CNRM-CM6-1	11 °C	∞ (12 ... ∞)	2.5 (1.3 ... 4.0)	12 (4.0 ... 3.3e+2)	2.0 (1.5 ... 2.6)
EC-Earth3	15 °C	∞ (1.1e+2 ... ∞)	5.9 (5.1 ... 6.6)	63 (26 ... 5.0e+2)	4.6 (4.2 ... 5.1)
EC-Earth3-Veg	13 °C	∞ (47 ... ∞)	3.0 (2.1 ... 3.9)	43 (18 ... 5.9e+2)	3.1 (2.6 ... 3.6)
INM-CM4-8	10 °C	1.4 (0.029 ... ∞)	0.16 (-1.3 ... 1.8)	1.9 (0.069 ... 12)	0.28 (-0.30 ... 0.79)
INM-CM5-0	12 °C	∞ (8.8 ... ∞)	2.2 (0.51 ... 3.8)	10 (0.00010 ... 2.5e+2)	1.4 (0.88 ... 1.9)
IPSL-CM6A-LR	7.3 °C	∞ (2.7 ... ∞)	0.90 (0.11 ... 1.8)	11 (4.5 ... 1.4e+2)	1.6 (1.3 ... 1.9)
MPI-ESM1-2-HR	11 °C	14 (0.75 ... ∞)	1.1 (-0.27 ... 2.2)	5.0 (1.9 ... 91)	0.94 (0.46 ... 1.5)
NorESM2-MM	11 °C	∞ (2.1 ... ∞)	2.2 (0.86 ... 3.5)	6.5 (2.3 ... 23)	1.2 (0.50 ... 1.9)
CNRM-CM6-1_r1i1p1f2	12 °C	3.6 (1.3 ... 1.2e+2)	1.5 (0.44 ... 2.9)	4.8 (1.7 ... 21)	1.7 (0.93 ... 2.7)
CNRM-CM6-1-HR_r1i1p1f2	10 °C	5.0e+3 (6.6 ... ∞)	2.5 (0.74 ... 3.9)	7.4 (2.7 ... 24)	1.9 (1.1 ... 2.7)
EC-Earth3P_r1i1p1f1	12 °C	1.8e+2 (4.1 ... ∞)	2.4 (0.96 ... 4.0)	3.9 (2.0 ... 11)	1.1 (0.64 ... 1.7)
EC-Earth3P-HR_r1i1p1f1	8.8 °C	1.9e+2 (1.2 ... ∞)	1.1 (0.059 ... 2.4)	6.3 (2.9 ... 12)	0.96 (0.43 ... 1.5)
HadGEM3-GC31-HM_r1i1p1f1	9.0 °C	12 (0.89 ... ∞)	1.2 (-0.061 ... 2.4)	5.1 (2.5 ... 17)	1.8 (1.2 ... 2.4)
HadGEM3-GC31-LM_r1i14p1f1	13 °C	9.3e+5 (8.9 ... ∞)	4.4 (2.5 ... 6.3)	12 (5.2 ... 40)	2.7 (2.1 ... 3.5)
MPI-ESM1-2-HR_r1i1p1f1	12 °C	5.6e+2 (3.9 ... ∞)	2.0 (0.82 ... 3.4)	2.9 (1.5 ... 11)	0.67 (0.26 ... 1.2)
MPI-ESM1-2-XR_r1i1p1f1	12 °C	∞ (46 ... ∞)	1.8 (0.77 ... 3.0)	8.2 (3.6 ... 18)	1.1 (0.60 ... 1.5)

1					
---	--	--	--	--	--

6 Hazard synthesis

We evaluate the influence of anthropogenic climate change on the TX7x-May event described above by calculating the probability ratio as well as the change in intensity using observation-based products and climate models. Models which do not pass the evaluation described above are excluded from the analysis. The aim is to synthesise results from models that pass the evaluation along with the observations-based products, to give an overarching attribution statement.

Figs. 6.1 and 6.2 show the changes in intensity and probability ratio for the observations (blue) and models (red). The results are also shown in Table 6.1. Before combining the results into a synthesised assessment, first, a representation error is added (in quadrature) to the observations, to account for the difference between observations-based datasets that cannot be explained by natural variability. This is shown in these figures as white boxes around the light blue bars. The dark blue bar shows the average over the observation-based products. Next, a term to account for intermodel spread is added (in quadrature) to the natural variability of the models. This is shown in the figures as white boxes around the light red bars. The dark red bar shows the model average, consisting of a weighted mean using the (uncorrelated) uncertainties due to natural variability plus the term representing intermodel spread (i.e., the inverse square of the white bars).

Observation-based products and models are combined into a single result in two ways. Firstly, we neglect common model uncertainties beyond the intermodel spread that is depicted by the model average, and compute the weighted average of models (dark red bar) and observations (dark blue bar): this is indicated by the magenta bar. As, due to common model uncertainties, model uncertainty can be larger than the intermodel spread, secondly, we also show the more conservative estimate of an unweighted, direct average of observations (dark blue bar) and models (dark red bar) contributing 50% each, indicated by the white box around the magenta bar in the synthesis figures.

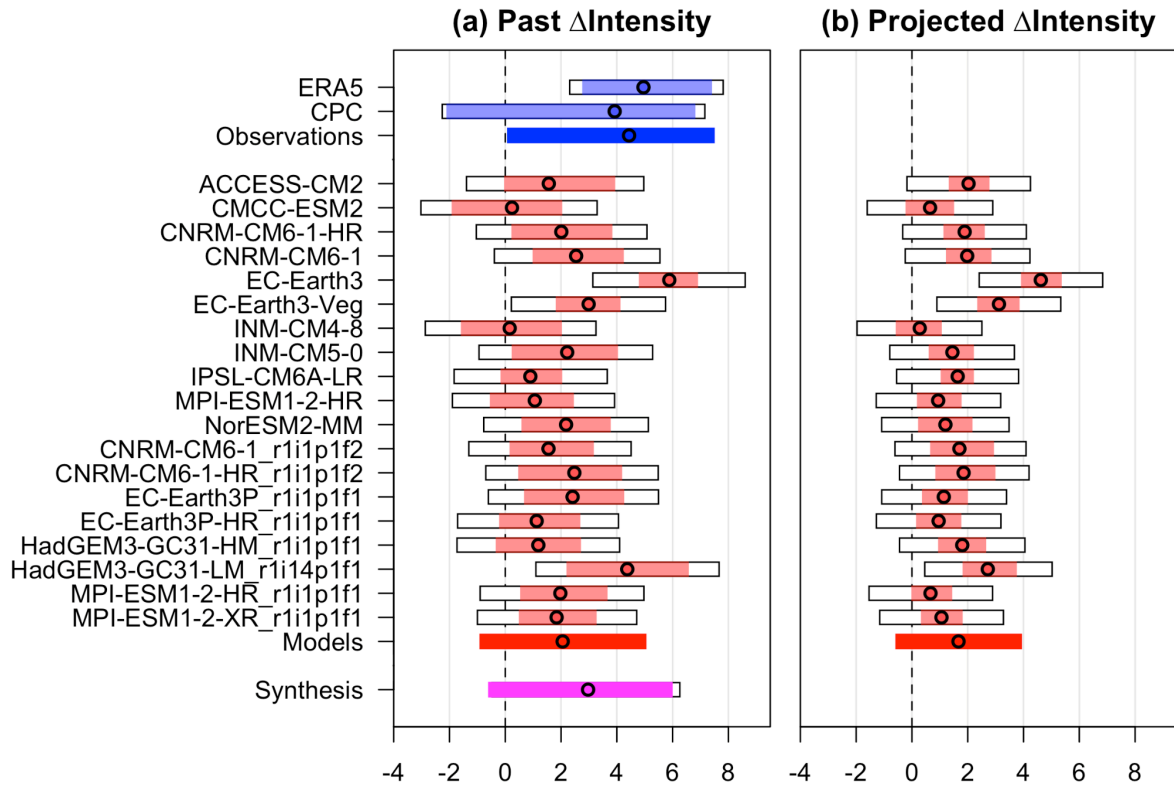


Figure 6.1: Synthesis of intensity changes of TX7x-May [$^{\circ}\text{C}$] over Iceland for (a) today's climate compared with a 1.3°C cooler climate and (b) a 2.6°C warmed climate (since the pre-industrial period) compared with today's climate.

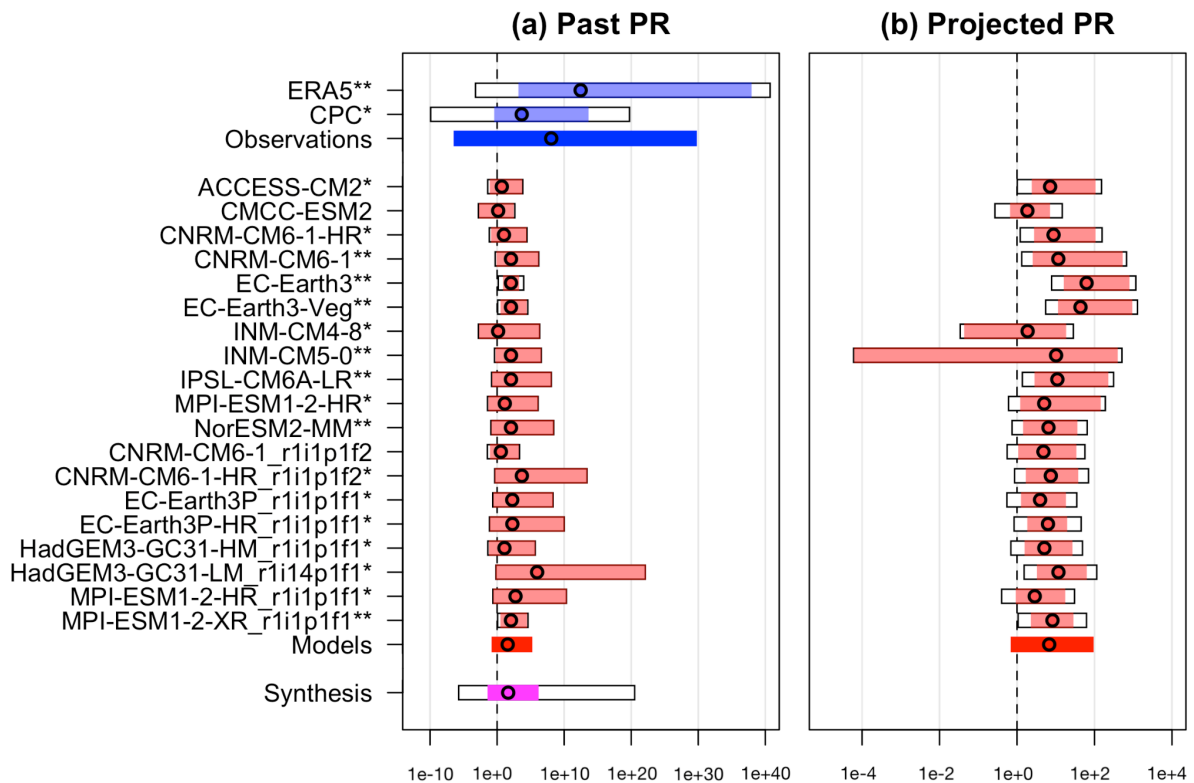


Figure 6.2: As for Fig. 6.1 but for Probability Ratio. Note that the x-axis range in a and b differs.

Turning first to changes in intensity of TX7x-May heat events over Iceland as a whole, the synthesis of the two gridded observational data sets gives a best estimate of 4.4°C (95%CI 0.35 to 7.2°C), the synthesis of the models gives a best estimate of around 2.1°C (95%CI -0.6 to 4.8°C) and observations and models combined gives a weighted synthesis (magenta bar) intensity change of 3.0°C (95%CI -0.3 to 5.7). Whilst large variability leads to large confidence intervals, there is clear agreement in the direction of change with all individual dataset best estimates showing positive changes, albeit with observational intensity changes being larger than most model results - a behaviour seen in heat studies in many areas of the world and particularly in Europe. The positive trend is projected to continue into the future, with models showing a further 1.7°C (95%CI -0.3 to 3.7°C) increase in the intensity of 7-day May heatwaves in a world 1.3°C warmer than now.

A similar picture emerges in changes in occurrence probability of 7-day heatwaves over Iceland with increases in probability in all individual datasets but again with models underestimating the probability ratio compared to observations. The synthesis of the models gives a PR of nearly 40 (95% CI: 2.3 to 12000) and the synthesis of observations gives a best estimate that is many orders of magnitude larger. Combining the observations and models, the weighted synthesis (magenta bar) gives a PR of about 45 (95%CI: 0.6 to 100,000). In a 1.3°C warmer future, models predict a further increase in frequency of 7-day May heatwaves - they become about 7 times (95% CI: 1.1 to 60 times) more likely compared to now. The models underestimate the observed trend, resulting in future projections that are too low compared to what we would expect from observations. That models struggle to accurately represent trends in extreme temperatures is a known problem ([van Oldenborgh et al., 2022](#)).

Also on the local scale there is clear evidence of intensification and increasing frequency of heat events in both Iceland and Greenland in observations. The analysis of Greenland synoptic station Ittoqqortoormiit shows an increase in intensity of 3.9°C and a PR of 110 (95%CI: >6), indicating that May single-day heat extremes – of the magnitude seen this year or greater – are occurring around 110 times more frequently now than in the past 1.3°C cooler climate. The Icelandic stations of Egilsstaðir airport and Reykjavik also show increases in intensity of 2.5°C (95%CI: -0.7 to 5.3°C) and 1.5°C (0.008 to 3.2°C) respectively. These are smaller magnitude changes than for Ittoqqortoormiit, but this does not imply that the warming is consistently greater in all Greenland compared to Iceland stations. Regional differences exist. Also it should be noted that records of daily mean temperature are longer and more thoroughly quality controlled in these Arctic regions than daily maximum (and minimum) temperatures, which have less meaning in the arctic winter when the diurnal cycle is absent in some regions.

Circulation analogues show that the type of circulation present during the May 2025 event has declined in frequency since 1950, indicating that the trend in heat extremes in the region is not due to an increase in this type of circulation. However when this type of circulation configuration occurs, it is associated with warmer temperatures now than in the past. While this particular pattern is linked with heat events over Iceland, the probabilistic attribution analysis however is not restricted to this type of circulation alone and it can include heat events from different circulation patterns that also contribute to the trend in extreme heat.

Combining lines of evidence from the synthesis results of the past climate, results from future projections showing continued trends, and physical knowledge of the presence of arctic amplification, we conclude that the 7-day May heat experienced in Iceland is about 3°C hotter due to human induced climate change and that the intensification of single-day May heat extremes observed at individual stations in Greenland and Iceland is evident and also largely driven by human induced climate change, and that thermodynamic processes likely play a larger role than changes in circulation dynamics in the

intensification of springtime heat extremes in the area.

Under current climate policies, extreme heat events like the one analyzed here are expected to become at least 2 °C hotter by the end of the century, and events of this magnitude will no longer be rare in a world that is 2.6 °C warmer than pre-industrial levels.

*Table 6.1: Summary of results for TX7x-May over Iceland, presented in Figs. 6.1-6.2. Statistically significant increases in probability and intensity are highlighted in dark orange, while non-significant increases are highlighted in light orange. Statistically significant changes are also highlighted in **bold font**.*

Data	GMST		
		Probability ratio (95% CI)	Intensity change [°C] (95% CI)
Observations	Past-Present	1.171E+8 (4.95E-6 to 4.20E+28)	4.439 (0.346 to 7.229)
Models		37.814 (2.254 to 12307)	2.0573 (-0.642 to 4.782)
Synthesis		45.234 (0.564 to 104065)	2.970 (-0.334 to 5.720)
Models only	Present-Future	6.777 (1.092 to 59.539)	1.670 (-0.314 to 3.665)

7 Vulnerability and exposure

Located in the North Atlantic and Arctic regions, respectively, Iceland and Greenland are geographically distinct yet climatically intertwined. Iceland, a volcanically active island nation, has a population of roughly 380,000, largely urbanized, with about 60% residing in the capital region of Reykjavik ([WHO, 2022](#); [Statistics Iceland, 2024](#)). Greenland, an autonomous territory within the Kingdom of Denmark, is the world's largest island but home to just 56,000-58,000 people - up to 90% of whom are Inuit, one of the few Indigenous Peoples with self-government, though still a minority within the Danish state ([IWGIA, n.d.](#); [Index Mundi, 2021](#)). Climate change is known to disproportionately affect Indigenous Peoples, who often rely directly on their environment to meet their basic needs ([Expert Mechanism on the Rights of Indigenous Peoples, 2019](#)). Towns and settlements in Greenland are dispersed along the coastline, and there are no roads between towns with most places accessible only by sea or air.

In mid-May 2025, a heatwave gripped parts of Iceland and Greenland. Temperatures in Iceland soared above 26C, record breaking for the month, prompting warnings from the Road Administration over bituminous bleeding on major roads, which is when too much asphalt comes up to the road surface making it shiny, sticky, and slippery ([RÚV, 2025](#)). Unlike previous heatwaves with similar maximum temperatures in June and July, this early-season event likely posed heightened risks due to lower physiological and behavioral acclimatization to heat. In the summer of 2021, similar heat (several consecutive days exceeding 20C) led to widespread snowmelt, river flooding, and animal distress, with reports of dogs burning their paws on hot asphalt and increased veterinary demand ([Maurer, 2021](#); [Icelandic Met Office, 2021](#)).

7.1 Heat risk

Although Iceland and Greenland are generally cold-climate regions with low historical exposure to extreme heat, recent trends suggest this is shifting. Reykjavik, for example, is one of Europe's lowest-risk cities for heat-related mortality ([Ignjacevic et al., 2024](#); [Di Napoli, Pappenberger & Cloke, 2018](#)), but under continued warming, deaths could rise from 3 to over 13 per 100,000 by 2080 under RCP8.5 ([WHO, 2022](#)). Vulnerability to heat is uneven across populations. Older adults, children, and individuals with chronic illness or limited access to healthcare are particularly at risk ([WHO, 2022](#); [Grigorieva, 2024](#)). Across both countries, health disparities by education and income are stark ([Index Mundi, 2021](#); [OECD, 2021](#); [OECD, 2019](#)). In Greenland, life expectancy is about a decade shorter than in Denmark and people suffer a greater prevalence of non-communicable disease, while most residents (over 80%) rely on subsistence food systems increasingly threatened by climate change ([Greenland Health Commission, 2023](#); [Minor et al., 2019](#)). These food systems face multiple stressors under climate change, including changes in species availability, access, and seasonal predictability. Meanwhile, Iceland's geothermal emissions contribute to air pollution, compounding health risks when combined with heat ([Bustaffa et al., 2020](#); [Finnbjornsdottir et al., 2016](#)). In both contexts, socioeconomic status, remoteness, and the adequacy of local health systems shape communities' capacity to cope with new and intensifying heat extremes ([World Bank, n.d.](#); [WHO, 2022](#)).

While Iceland and Greenland differ significantly in development and access to basic services, the functioning and resilience of essential infrastructure strongly shape how communities experience and respond to heat. In Iceland, well resourced public systems - including universal healthcare and affordable energy - help buffer the impacts of heat extremes, supporting access to cooling and medical care even during periods of elevated demand ([Statista, 2023](#); [Halldorsdottir et al., 2023](#)). In Greenland, vulnerabilities are more pressing, particularly in rural and remote areas. During the extreme heat and rainfall of August 2022, widespread permafrost thaw led to the release of iron and other metals into thousands of Arctic lakes, raising concerns over water quality and carbon feedbacks ([Saros et al., 2025](#)). Sanitation infrastructure remains unevenly developed: while urban centers have piped systems, about 90% of rural households rely on bag toilets disposed of in open dumps, increasing health risks, especially under warmer conditions that accelerate bacterial growth ([Hendriksen & Hoffman, 2017](#)). The health system in Greenland is already under historic pressure due to aging facilities, a significant aging population, increased tourism, and persistent understaffing ([Greenland Health Commission, 2023](#)). These disparities highlight how infrastructural inequalities intersect with climate hazards to shape differential exposure and coping capacity across the region.

National patterns of vulnerability intersect with localized dynamics, particularly in urban environments where population density and built infrastructure can amplify heat exposure - even under moderate temperature extremes.

7.2 Urban exposure to heat

Research is growing in recent years on cold and polar urban climate impacts, however Iceland and Greenland are underrepresented in research as geographical outliers ([Brozovsky et al., 2021](#)). Moreover, studies tend to overlook human impacts, making it difficult to identify vulnerability and exposure factors ([Hanibal & Wadling, 2023](#)). The existing evidence from other urban areas in the arctic circle shows, while absolute temperatures of heatwave events are relatively low compared to other geographies in lower latitudes, Urban Heat Island effects are still present and heat-related mortality can occur ([Esau et al., 2021](#), [Grigorieva, 2024](#)). For instance, evidence from sub-arctic cities in Russia suggests increased mortality among elderly population groups in heatwaves with temperatures of just 20-23°C ([Revich & Shaposhnikov, 2022](#)). It should be noted however that urban areas with lower temperatures during heatwave events showed no significant effect on mortality.

While heat related deaths are low in Iceland, urbanisation alongside increasing urban heat island effect is expected to increase the likelihood of adverse health impacts of heatwaves among the most vulnerable in Iceland's population ([WHO, 2022](#)). In Iceland's capital Reykjavik, land surface temperatures have risen by 67.5% between 1987 and 2020 already and are expected to increase further by 2030 ([Mansourmoghaddam et al., 2023](#)).

While Iceland and Greenland are among the least densely populated countries, the majority resides in few urban centers. 88% of Greenland's population and 94% of Iceland's population live currently in urban centers ([World Bank, 2023](#)). Hence, large parts of the total population are potentially exposed to future urban heatwave impacts affecting health and infrastructure. For example, increased melting of ice during heatwaves has been linked to flooding and destruction of roads and infrastructure repeatedly between 2012-2024 in Greenland ([Shin, 2024](#)). In Iceland, the high temperatures have

softened road pavements, making it stick to the vehicles tires and absorbing anti-slip agents in the road, increasing risk for accidents ([Guðmundsdóttir, 2025](#)).

In the current heatwave, direct impacts on the population have not been reported in urban areas in Iceland or Greenland. Yet, heat-related deaths in Iceland are expected to increase in the future ([WHO, 2022](#)). In Greenland, vulnerable populations might face heightened risk of adverse impacts as well. Despite well planned urban development and no informal/unregulated housing, homelessness is becoming increasingly a challenge in the Arctic region, particularly in Greenland's capital Nuuk, due to a mix of factors including the impacts of colonial policies ([Cullen, 2025](#)), unevenly distributed resources, and changing demographics and labour market demands in urban areas, exposing them to harsh living conditions and potentially adverse impacts of heatwaves ([Christensen & Arnfjord, n.d.](#)). Heat related health risk tends to be exemplified among people experiencing homelessness compared to the general population, although Greenland specific insights are missing ([Noor et al., 2025](#))

Beyond cities, the impacts of heatwaves ripple across ecological, hydrological, and socio-economic systems, especially in fragile Arctic environments where small temperature shifts can trigger broad cascading effects.

7.3 Compounding and cascading risks

In recent decades, the Arctic has been warming nearly four times faster than the global average ([Rantanen et al., 2022](#)) - a phenomenon known as Arctic amplification. This acceleration drives profound ecological and societal change. In Greenland, permafrost thaw destabilized infrastructure and increases risks of landslides and landslide-induced tsunamis ([Matti et al., 2023](#)), while the increasing unpredictability, thinning, and shortening duration of sea ice seasons threatens Indigenous mobility, hunting, and food sovereignty ([IPCC / Meredith et al 'Polar Regions' 2019, p 205](#); [Cullen & Witjes, 2024](#); [Minor et al., 2019](#); [Somme et., al 2018](#)). It can also disrupt scientific fieldwork ([Sterna Paradisaea, 2025](#)). Under high-emissions scenarios (RCP8.5), average annual temperatures could rise by nearly 4C in the Arctic by 2100, with “hot days” (exceeding the 90th percentile) increasing from 15% to approximately 50% of all days ([WHO, 2022](#)). The attribution analysis shows that climate change has already made studied heatwave roughly 3C hotter and up to 40 times more likely.

A prolonged period of unseasonal warmth, such as the given heatwave with maximum temperatures exceeding 20C over ten consecutive days ([Icelandic Met Office, 2025](#)), can trigger a range of compounding and cascading risks across socio-ecological systems in the Arctic. In agriculture, early and sustained heat can stress cold-adapted crops and intensify pest activity, potentially reducing yields. While warmer temperatures may enhance productivity in select Icelandic regions, benefits are uneven and vulnerable to variability ([WHO, 2022](#)). Hydrologically, rapid snow and ice melt increases river discharge, heightening flood risk and complicating reservoir and catchment management, particularly in mountainous areas where spring runoff is already seasonally sensitive.

As sea surface temperatures shift, species distributions change. While some fisheries benefit from the increased presence of cod and mackerel, the displacement of cold-water species like shrimp and halibut toward northern waters introduces spatial and economic strain ([Shankman, 2019](#)). Additionally, warming leads to increased seaweed proliferation and compromised fodder availability.

Greenlandic farmers have been forced to import hay from Iceland, raising operational costs and exposing cross-border dependencies.

These interlinked risks underscore the systemic nature of springtime heat extremes in high-latitude environments, where early warmth can destabilize ecosystems, livelihoods, and infrastructure in compounding ways. Understanding the state of heat risk governance across the countries sheds light on adaptive capacities and remaining gaps.

7.4 Heat risk governance

Iceland's early warning system, managed by the Icelandic Meteorological Office (IMO), uses the Common Alerting Protocol (CAP) to issue standardized, color-coded, impact-based alerts for hazards driven by wind and precipitation. While heat is not included as an official alert category, IMO does communicate heat risk via media, including warnings on UV exposure and related health risks as well as increased risk for wildfires ([RÚV, 2025a](#); [RÚV, 2025b](#); [Icelandic Met Office, 2025](#)). Iceland lacks a dedicated heat-health action plan, but ongoing work aims to integrate health-specific responses into its broader risk management strategies ([WHO, 2022](#)). The relatively low level of institutional integration of heat risk to date reflects its historically limited public health burden. Reykjavik has been ranked among the European cities with the lowest projected heat-related mortality, and past exposure to extreme heat has been rare and of short duration ([Ignjacevic et al., 2024](#); [Di Napoli, Pappenberger & Cloke, 2018](#); [WHO, 2022](#)).

Greenland does not yet have a formal heat early warning system nor heat-health action plan. Early warning systems are being developed for other hazards, such as glacial meltwater floods and ice sheet runoff, but community-level implementation remains limited ([Nation CYMRU, 2025](#); [Jex, 2017](#)). While climate-related health risks are increasingly acknowledged in Greenlandic health policy, heat has not yet emerged as a distinct focus within national adaptation or resilience planning ([Greenland Health Commission, 2023](#)). This limited integration may be influenced by a lack of heat-specific epidemiological data or health risk projections for Greenland. Compared to other Arctic nations, Greenland appears underrepresented in research on heat exposure and associated health outcomes, likely reflecting its colder climate baseline and the relatively early stage of climate-health surveillance efforts ([Hanibal & Wadling, 2023](#)). At the same time, future research efforts must avoid what the Sami call "green colonialism" in which Indigenous People's rights are infringed in the name of a green transition, including scientists who are extractive and fail to ensure proper free, and prior informed consent of locals ([Olsvig and Cullen, 2024](#)).

Both countries reflect the broader Arctic trend - rising temperatures are beginning to challenge current institutional preparedness. While Iceland is incrementally adapting its existing systems, Greenland remains in the early stages of recognizing and responding to heat as a public health threat.

7.5 V&E conclusions

Heatwaves are relative. In Greenland and Iceland with fairly low average temperatures year-round, even 26C is unusual for people and infrastructure that is adapted and reliant on colder temperatures.

Heat can impact road infrastructure, agriculture, water availability, sea ice extent and related livelihoods (e.g. fishing). While heat impacts to human health in the region tend to focus on risks associated with sunburns, rather than other more serious heat related illnesses, these are expected to grow as the climate continues to warm. Furthermore, differences between the two countries in terms of infrastructure (including social) and healthcare result in different coping capacities as climate change continues to drive hotter temperatures. While currently a nascent risk, this analysis points to more frequent and intense heat extremes already, providing a warning to prepare for this trend to continue into the future and potentially expand health impacts.

Data availability

All time series used in the attribution analysis are available via the Climate Explorer.

References

All references are given as hyperlinks in the text.